Neutrino Mass and Oscillation : An Introductory Review[*]

D.P. Roy

Tata Institute of Fundamental Research

Homi Bhabha Road, Colaba

Mumbai - 400 005, INDIA

Abstract

After a brief introduction to neutrino mass via the see-saw model I discuss neutrino mixing and oscillation, first in vacuum and then its matter enhancement. Then the solar and atmospheric neutrino oscillation data are briefly reviewed. Finally I discuss the problem of reconciling hierarchical neutrino masses with at least one large mixing, as implied by these data. A minimal see-saw model for reconciling the two is discussed.

---

[*] Invited talk at the Symp. on Frontiers of Fundamental Physics, Hyderabad, 30 December 98 - 1 January 99 and the Discussion Meeting on Recent Developments in Neutrino Physics, Ahmedabad, 2-4 February 99.

Neutrino Mass : See-saw Model

The fermion masses are represented by the combination of Dirac spinors

$$m\bar{u}_L u_R, \tag{1}$$

while

$$\bar{u}_L u_L = \bar{u}_R u_R = 0. \tag{2}$$

It follows from the basic anticommutation relation of Dirac γ matrices that the bar of a left-handed projection operator is right-handed, so that the product of the opposite projection operators vanish identically. In the Standard Model (SM) the left-handed fermions occur in $SU(2)$ doublets and the right-handed ones in singlets except that there is no right-handed neutrino, i.e.

$$\begin{pmatrix} u_i \\ d_i \end{pmatrix}_L, u_{iR}, d_{iR}; \ \begin{pmatrix} \ell_i \\ \nu_i \end{pmatrix}_L, \ell_{iR}. \tag{3}$$

Here the particle labels represent the corresponding spinors and i is the generation index. Thus we can not have direct mass terms even for quarks and charged leptons, since terms like $m\bar{\ell}_L \ell_R$ are not gauge invariant. However they can acquire mass by absorbing the Higgs scalar ϕ, which is a $SU(2)$ doublet. Thus the Yukawa interaction, $f\phi\bar{\ell}_L \ell_R$, is gauge invariant. As the gauge symmetry is spontaneously broken, ϕ acquires a vacuum expectation value and correspondingly the fermion acquires a mass, i.e.

$$f\phi\bar{\ell}_L \ell_R \rightarrow \underbrace{f\langle\phi\rangle}_{m} \bar{\ell}_L \ell_R. \tag{4}$$

However this is not possible for the neutrino, since it does not have a right-handed component in the SM.

The simplest and most popular way of giving mass to the neutrino is via the see-saw model [1]. It assumes each neutrino to have a right-handed singlet component N_R like the other fermions. Unlike the latter however the N_R has a unique property. Its gauge charges corresponding to the SM gauge groups

$$SU(3)_C \times SU(2) \times U(1)_Y \tag{5}$$

are all zero — it carries no colour, isospin or hypercharge. It is called a Majorana particle, since the particle and antiparticle have the same gauge charges — minus zero is zero. Of course they have opposite lepton numbers, which is however not a gauge quantum number and hence need not be conserved. Consequently one can have a direct mass term coupling the right-handed singlet neutrino with its left-handed antiparticle,

$$M\overline{N_L^C}N_R, \tag{6}$$

which is called Majorana mass. This can be very large since it does not break any gauge symmetry. In addition one can have a Dirac mass term like (4), i.e.

$$m\bar{\nu}_L N_R. \tag{7}$$

Diagonalising the resulting mass-matrix in the $\nu_L - N_R$ basis induces a tiny mass for the left-handed neutrino, i.e.

$$\begin{pmatrix} 0 & m \\ m & M \end{pmatrix} \to \begin{pmatrix} m^2/M & 0 \\ 0 & M \end{pmatrix}. \tag{8}$$

The larger the Majorana mass of N_R the smaller will be the left-handed neutrino mass induced by it, since $m_\nu = m^2/M$. Therefore it is called see-saw model. It is an ingenuous model that solves two puzzles at one stroke. The large Majorana mass M banishes the right-handed neutrino beyond observation. It also makes the left-handed neutrino mass tiny compared to the other fermion masses, which are characterised by the Dirac mass m.

The way the Majorana mass (6) was introduced above as a direct mass term was rather adhoc. This was remedied in [2] by assuming an extension of the SM gauge group (5) by a

$$U(1)_{B-L}, \tag{9}$$

whose gauge charge corresponds to the difference of Baryon and Lepton numbers. In this case the requirement of anomaly cancellation implies the existence of 3 right-handed singlet neutrinos as in the case of the other fermions. This will ensure vector coupling of the $U(1)_{B-L}$ current as the axial parts cancel between the left and right handed fermions. Then one can easily see that the remaining axial anomalies cancel one by one. Therefore the $U(1)_{B-L}$ can be treated as a gauge symmetry along with the other symmetry groups of the SM. One assumes spontaneous breaking of this gauge symmetry at a high mass scale via a Higgs scalar χ, carrying 2 units of lepton number (i.e. $B - L = 2$). The coupling of this Higgs scalar leads to the Majorana mass

$$f\chi \overline{N_L^C} N_R \to \underbrace{f\langle\chi\rangle}_{M} \overline{N_L^c} N_R, \tag{10}$$

analogous to the Dirac mass (4). This is a left-right symmetric model, which can be embeded in $SO(10)$ GUT. Indeed all the fermions of one generation, including N_R, can be naturally accommodated in the 16 dimensional representation of $SO(10)$. In the $SU(5)$ GUT on the other hand the $10 + 5$ dimensional representation can naturally accommodate all the SM fermions of one generation. In this sense the $SU(5)$ GUT is more appropriate for the SM. But even in this case one can add a N_R as a $SU(5)$ singlet if needed. It may be noted here that in $SU(5)$ GUT one has the flexibility of adding any number of right-handed singlet neutrinos — not necessarily three. In fact we shall see later that a minimal solution to the atmospheric and solar neutrino oscillation data requires only two right handed singlet neutrinos.

Neutrino Mixing and Oscillation (Vacuum) :

If the neutrinos have nonzero mass, there will in general be mixing between the neutrino species as in the case of quarks. For most practical applications it is adequate to consider mixing between a pair of neutrino species, e.g.

$$\begin{pmatrix} \nu_e \\ \nu_\mu \end{pmatrix} = \begin{pmatrix} \cos\theta & \sin\theta \\ -\sin\theta & \cos\theta \end{pmatrix} \begin{pmatrix} \nu_1 \\ \nu_2 \end{pmatrix}, \tag{11}$$

where $\nu_{1,2}$ are the mass eigen states with eigen values $m_{1,2}$. Each of them propagates with a distinct phase factor, characterised by its mass. To see this we make the extreme relativistic approximation, appropriate for the tiny neutrino masses, i.e.

$$E_{1,2} \simeq p + m_{1,2}^2/2p \text{ and } t \simeq \ell. \tag{12}$$

Then the phase factors for the free particle wave functions of $\nu_{1,2}$ are given by

$$e^{-i(E_{1,2}t - p\ell)} \simeq e^{-\frac{im_{1,2}^2 \ell}{2E}}. \tag{13}$$

This automatically leads to neutrino oscillation [3] as we see below.

Let us consider a beam of ν_e produced at the origin. It can be split into the ν_1 and ν_2 components, each propagating with its own phase, i.e.

$$\nu_e \rightarrow \nu_1 \cos\theta e^{-\frac{im_1^2 \ell}{2E}} + \nu_2 \sin\theta e^{-\frac{im_2^2 \ell}{2E}}. \tag{14}$$

To find the ν_μ component in this beam after a certain distance ℓ, we split $\nu_{1,2}$ back to $\nu_{e,\mu}$, i.e.

$$\nu_e \rightarrow (\cos\theta\nu_e - \sin\theta\nu_\mu)\cos\theta e^{\frac{-im_1^2 \ell}{2E}}$$

$$+ (\sin\theta\nu_e + \cos\theta\nu_\mu)\sin\theta e^{\frac{-im_2^2 \ell}{2E}}. \tag{15}$$

Clearly the coefficient of the ν_μ term is nonzero. The square of this co-efficient represents the oscillation probability, i.e.

$$P_{\nu_e \rightarrow \nu_\mu}(\ell) = \left| \cos\theta\sin\theta \left(-e^{\frac{-im_1^2 \ell}{2E}} + e^{\frac{-im_2^2 \ell}{2E}} \right) \right|^2$$

$$= \sin^2 2\theta \sin^2 \frac{\delta m^2 \ell}{4E}, \tag{16}$$

where $\delta m^2 = m_1^2 - m_2^2$ and the two factors represent the amplitude and the phase of oscillation. Converting to more convenient units, one gets

$$P_{\nu_e \rightarrow \nu_\mu}(\ell) = \sin^2 2\theta \sin^2 \left(1.3 \underbrace{\delta m^2}_{eV^2} \cdot \underbrace{\ell}_{m} / \underbrace{E}_{MeV} \right)$$

$$= \sin^2 2\theta \sin^2(\ell\pi/\lambda), \tag{17}$$

where λ represents the wave length of oscillation. Note that the oscillation probability reaches maxima at odd multiples of

$$\lambda/2(m) = 1.25E(\text{MeV})/\delta m^2(\text{eV}^2), \tag{18}$$

4

while it vanishes at the even multiples. Thus for large mixing angle, $\sin 2\theta \simeq 1$, one can identify three distinct distance scales of oscillation, i.e.

$$\ell \qquad \ll \lambda/2 \simeq \lambda/2 \gg \lambda/2$$

$$\frac{P_{\nu_e \to \nu_\mu}(\ell)}{(1 - P_{\nu_e \to \nu_e}(\ell))} \;=\; \begin{matrix} 0 & 1 & 1/2, \end{matrix} \qquad (19)$$

where the last quantity comes from averaging P.

It is clear from the above discussion that assuming large mixing one can see the effect of neutrino oscillation for

$$\ell(m) \gtrsim 1.25 E(\text{MeV})/\delta m^2(\text{eV}^2), \qquad (20)$$

and the same relation holds if we replace the units of distance and energy by Km and GeV respectively. Let us illustrate this with some real life examples.

Table I. Sensitivity of different types of neutrino experiments
to the scales of neutrino mass

ν Source	Energy (E)	Dist. (ℓ)	δm^2
Reactor	$\sim$ MeV	$10^2 \ m$	$\gtrsim 10^{-2}$ eV^2
Sun	-"-	$10^{11} \ m$	$\gtrsim 10^{-11}$ eV^2
Accelerator	$\sim$ GeV	Km	$\gtrsim$ eV^2
Atmosphere	-"-	10^4 Km	$\gtrsim 10^{-4}$ eV^2

Table I summarises the typical energy and distance scales for the four different types of neutrino experiments. The reactor and solar neutrinos, arising from nuclear reactions, have energies in the MeV range. The typical distance travelled is $\sim 10^2$ meters in the former case and 1 AU $\simeq 10^{11} \ m$ in the latter. Thus from (20) the reactor neutrino oscillation experiments are sensitive to $\delta m^2 \gtrsim 10^{-2}$ eV^2 while the solar neutrino oscillation is sensitive down to 10^{-11} eV^2. The accelerator and atmospheric neutrinos, arising from pion decay in flight, have typical energies in the GeV range. The typical distance scale for short base line accelerator neutrino experiments is ~ 1 Km, while it is $\sim 10^4$ Km for atmospheric neutrinos traversing through the diameter of the earth. Thus the accelerator neutrino oscillation experiments are sensitive to $\delta m^2 \gtrsim$ eV^2, while atmospheric neutrino oscillation is sensitive down to 10^{-4} eV^2.

Of course the above realisation is not new. Soon after the discovery of neutrino, it was observed by Pontecorvo [3] that the solar neutrino oscillation experiment can probe for neutrino mass down to a small fraction of an eV, if there is significant mixing between the neutrino species. Indeed this provided the main motivation for starting the solar neutrino experiment in the late sixties. Later on it was realised that the solar neutrinos can show large oscillation even for small mixing between the neutrino species [4-6], as we see below.

Matter Enhancement (Resonce Oscillation) :

This phenomenon is also known as the MSW effect, as it was systematically worked out by Mikheyev and Smirnov [4] following the original suggestion of Wolfenstein [5]. This is

analogous to the effect of the medium on the propagation of light, which imparts an induced mass to the photon, resulting in the index of refraction. Similarly the neutrino, propagating through the sun, acquires an induced mass.

The electrons in the solar medium has charged current interaction with ν_e,

$$\nu_e e \xrightarrow{W} e\nu_e, \tag{21}$$

but not with ν_μ or ν_τ. The resulting interaction energy is given by

$$H_{\text{int}} = \sqrt{2}G_F N_e, \tag{22}$$

where G_F and N_e are the Fermi coupling and the electron density in the solar medium. The corresponding neutral current interactions are identical for all neutrino species and hence have no net effect on their propagation. To see the effect of the charged current interaction let us consider the wave equation for ν_e and ν_μ as in the last section, but now including the interaction energy (22). We have

$$-\frac{id}{dt}\begin{pmatrix} \nu_e \\ \nu_\mu \end{pmatrix} = \left(p + \frac{M^2 + 2pH_{\text{int}}}{2p}\right)\begin{pmatrix} \nu_e \\ \nu_\mu \end{pmatrix}. \tag{23}$$

Defining the quantity

$$M'^2 = M^2 + 2pH_{\text{int}} \simeq M^2 + 2EH_{\text{int}}, \tag{24}$$

as an effective mass or energy, we see that

$$\begin{aligned}
M'^2 &= \begin{pmatrix} c & s \\ -s & c \end{pmatrix}\begin{pmatrix} m_1^2 & 0 \\ 0 & m_2^2 \end{pmatrix}\begin{pmatrix} c & -s \\ s & c \end{pmatrix} + \begin{pmatrix} 2\sqrt{2}EG_F N_e & 0 \\ 0 & 0 \end{pmatrix} \\
&= \begin{pmatrix} c^2 m_1^2 + s^2 m_2^2 + 2\sqrt{2}EG_F N_e & sc\delta m^2 \\ sc\delta m^2 & c^2 m_2^2 + s^2 m_1^2 \end{pmatrix},
\end{aligned} \tag{25}$$

where s, c denote $\sin\theta, \cos\theta$. The 1st term represents the squared neutrino masses, rotated into the flavour basis, while the 2nd term represents the interaction energy (22).

Let us consider small mixing angle, $s \ll 1$, so that the eigen states of (25) correspond approximately to the flavour eigen states ν_e and ν_μ. The corresponding eigen values are shown against the electron density in Fig. 1 for the case $m_2 > m_1$. They roughly correspond to the two diagonal elements of (25). At the solar surface $N_e \to 0$, so that the energy eigenvalues of ν_e and ν_μ correspond to their masses. As one goes towards the solar core, however, the eigen value of ν_e increases with N_e and ultimately overtakes that of ν_μ. The two energy levels cross over at $M_{11}'^2 = M_{22}'^2$, i.e.

$$N_e^c = \frac{\delta m^2}{2\sqrt{2}G_F E}\cos 2\theta. \tag{26}$$

Of course the finite off-diagonal elements ensure that the two energy levels are separated at this point by a small but finite gap

$$\Gamma = \delta m^2 \sin 2\theta, \tag{27}$$

6

which represents the width of the energy interval over which the level crossing takes place. In analogy with vacuum oscillation, one can define an effective mixing angle in matter as

$$\tan 2\theta_M = \frac{2M_{12}'^2}{M_{22}'^2 - M_{11}'^2} = \frac{\sin 2\theta}{\cos 2\theta - 2\sqrt{2}EG_F N_e/\delta m^2}. \tag{28}$$

No matter how small the mixing angle θ the resonance condition (26) ensures that $\theta_M \to 45°$ at the cross-over point. This is why it is called matter enhanced (or resonant) oscillation.

Physically speaking, the ν_e produced at the solar core has an energy level higher than that of ν_μ (Fig. 1). It continues to occupy this higher energy level as it emerges through the region of critical density N_e^c, which means that it emerges out as ν_μ. This assumes of course that the transition probability between the two energy levels at the critical point remains small, i.e.

$$T \propto \gamma_c^{-1} \propto \frac{2E}{\delta m^2} \frac{\cos 2\theta}{\sin^2 2\theta} \left(\frac{dN_e/d\ell}{N_e}\right)_c \ll 1. \tag{29}$$

This is called the adiabatic condition. One can show from (18), (26) and (27) that the above expression represents the ratio of the oscillation wave-length λ to the distance over which the energy eigen value changes by an amount Γ. Thus the adiabatic conditon (29) requires the N_e to change very slowly during the level crossing, so that the resulting change in the energy over a distance λ is $\ll \Gamma$ [6]. Such a slow change of energy ensures that the wave function continuously adjusts itself to one energy level (upper or lower) in stead of jumping to the other.

Thus the twin conditions for the resonant conversion of $\nu_e \to \nu_\mu$ inside the sun are $N_e^o > N_e^c$ and the adiabatic condition (29). Quantitively speaking the conditions for $\geq 50\%$ conversion of solar neutrino,

$$\langle P_{\nu_e \to \nu_e}\rangle < 0.5 \tag{30}$$

are

$$\frac{\delta m^2 \cos 2\theta}{2\sqrt{2}G_F N_e^o} < E < \frac{\pi \delta m^2 \sin^2 2\theta}{4\ell n2 \cos 2\theta (N_e^{-1}dN_e/d\ell)_c}. \tag{31}$$

The 1st inequality ensures resonant transition by requiring that the core density is higher than the critical density of (26), while the 2nd ensures the adiabatic condition (29) [7].

One clearly expects from (31) a nonmonotonic suppression of the solar ν_e flux as a function of neutrino energy, with the maximum suppression occuring for some value of E in between the two limits. As we shall see in the next section, this pattern seems to be observed in the Gallium, Chlorine and the Water-Cherenkov experiments, which are in increasing order of neutrino energy (see Fig. 2 and Table II). While the Gallium and the Water-Cherenkov experiments show a suppression rate $\langle P_{\nu_e \to \nu_e}\rangle \simeq 0.5$, the chlorine experiment shows a higher suppression rate of $\simeq 0.3$.

Finally, one sees from (30) and (31) that when a solar neutrino experiment, corresponding to particular range of E, finds a suppression rate for the solar ν_e flux, the result can be cast into a contour plot in the $\delta m^2 - \sin^2 2\theta$ plane. These contours are generally of triangular shape, as seen in Fig. 3. To understand why let us concentrate on the contour for the Gallium experiments (SAGE and GALLEX), corresponding to $\langle E \rangle \simeq 0.5$ MeV and $\langle P_{\nu_e \to \nu_e}\rangle \simeq 0.5$. The resonance condition of (31) fixes the δm^2 value, roughly independent of $\sin^2 2\theta$, resulting

in the horizontal side of the triangle. The adiabatic condition implies a minimum value of the mixing angle, $\sin^2 2\theta \gtrsim 10^{-3}$. At the large angle end both the conditions of (31) are satisfied, so that there is complete MSW conversion between the two neutrino species. Consequently

$$\langle P_{\nu_e \to \nu_e} \rangle = \sin^2 \theta, \text{ i.e. } \sin^2 2\theta = 4\langle P \rangle (1 - \langle P \rangle), \tag{32}$$

which corresponds to the vertical side. It extends downward by 3 orders of magnitude in δm^2, at which point the adiabatic condition ceases to holds. The third side corresponds to the non-adiabatic solution to eq. (23). Assuming a constant density gradient, $dN_e/d\ell$, one gets [8]

$$\langle P_{\nu_e \to \nu_e} \rangle \sim e^{-\pi \gamma_c / 2}. \tag{33}$$

This corresponds to a contour of fixed $\delta m^2 \sin^2 2\theta$, i.e. a diagonal line in the $\log \delta m^2 - \log \sin^2 2\theta$ plot (see eq. 29).

Solar Neutrino Oscillation :

The main sources of solar neutrinos are the three pp chains of nuclear reactions, taking place at the solar core, which convert protons into ^4He (α particle). They are

(I) $pp \to^2 H + e^+ + \nu_e,\ ^2H + p \to^3 He + \gamma,\ ^3He +^3 He \to^4 He + 2p$; or

(II) $^3He +^4 He \to^7 Be + \gamma,\ ^7Be + e^- \to^7 Li + \nu_e,\ ^7Li + p \to 2^4He$; or

(III) $^7Be + p \to^8 B + \gamma,\ ^8B \to^8 Be^\star + e^+ + \nu_e,\ ^8Be^\star \to 2^4He.$ (34)

While most of this conversion takes place by the straight path (I) a small fraction takes place through a detour via ^7Be (II) and a still smaller one through a longer detour via ^8B (III). Thus the pp neutrino has the highest flux, followed by those of ^7Be and ^8B neutrinos. But their energies are in reverse order. These are shown in Fig. 2, along with the energy ranges of various solar neutrino experiments [9]. The Gallium experiment gets largest contribution from pp neutrino (55%), followed by the ^7Be (25%) and ^8B (10%) neutrinos. The chlorine experiment gets largest contribution from ^8B neutrino (75%) followed by the ^7Be (15%). The remainder in both cases come from the pep and the CNO neutrinos. The water Cherenkov experiment gets contribution only from the ^8B neutrino.

The Gallium [10] and the Chlorine [11] experiments are based on the reaction

$$\nu_e +^{71} Ga \to e^- +^{71} Ge, \tag{35}$$

$$\nu_e +^{37} Cl \to e^- +^{37} Ar. \tag{36}$$

The produced ^{71}Ge and ^{37}Ar are separated by radio chemical method, from which the neutrino fluxes are estimated. On the other hand the water Cherenkov experiments are based on the charged current interaction (21), where the outgoing electron is detected by its Cherenkov radiation. Thus it is a real time experiment. It also has directionality; the direction of the incoming neutrino can be estimated from that of the outgoing electron. Thus one can study day-night (Zenith angle) variation of solar ν_e flux, which probes the effect of its propagation through earth. Similarly the energy spectrum of the incoming neutrino can also

be estimated from that of the outgoing electron. It may be noted here that this experiment also gets a contribution from the Neutral Current reaction,

$$\nu_{e,\mu} + e^- \xrightarrow{Z} \nu_{e,\mu} + e^-; \tag{37}$$

but at a reduced sensitivity of about 1/6th of the charged current process.

Table II. The threshold energies of different solar neutrino experiments along with the predicted and observed ν_e fluxes (in $10^6 \ cm^{-2}s^{-1}$ units) for the Kamiokande and event rates (in solar neutrino units) for the others. Their ratio gives the survival probability shown in the last column.

Expt.	Target	E_{th}(MeV)	Pred.	Obs.	$\langle P_{\nu_e \to \nu_e} \rangle$
GALLEX [10]	Gallium	0.2	129^{+8}_{-6}	78 ± 8	$0.60 \pm .07$
SAGE [10]	-"-	-"-	-"-	67 ± 8	$0.52 \pm .07$
Homestake [11]	Chlorine	0.8	$7.7^{+1.2}_{-1.0}$	$2.56 \pm .23$	$0.33 \pm .05$
Kamiokande [12]	Water	7.5	$5.15^{+1.0}_{-0.7}$	$2.80 \pm .38$	$0.54 \pm .07$
Super-Kamiokande [12]	-"-	6.5	-"-	$2.44 \pm .10$	$0.47 \pm .08$

Table II lists the threshold energies of different solar neutrino experiments along with the theoretically predicted and experimentally observed results. The ratio of the two corresponds to the ν_e survival probability (supression rate) $\langle P_{\nu_e \to \nu_e} \rangle$, shown in the last column. As mentioned in the last section, one can clearly see the nonmonotonic energy dependence of this probability, as suggested by the MSW solution. It should be noted here that Kamiokande values for this quantity will go down further by ~ 0.1 unit after taking account of the neutral current interaction (37) effect.

The MSW solutions to the observed suppression rates $\langle P_{\nu_e \to \nu_e} \rangle$ for the 3 sets of experiments are shown in Fig. 3 [13]. As discussed in the last section, each solution corresponds to a triangular region in the $\delta m^2 - \sin^2 2\theta$ plane. The vertical position of each triangle scales with the average neutrino energy of the corresponding experiment (see eq. 31). The overall solution to the observed suppression rates corresponds to the overlap region among the triangles, which are shown by the two shaded areas. They represent the small and large angle MSW solutions. The additional constraints coming from the Kamiokande energy spectrum and day-night effect are also indicated. However, they do not impinge upon the two allowed regions. Fig. 4 shows a more recent MSW analysis of the solar neutrino data including the latest Super-Kamiokande results [14]. While one can have both the small and large angle solutions to the rates and energy spectrum, only the small angle solution survives after including the zenith angle distribution.

Finally Fig. 5 shows the corresponding vacuum oscillation solution to the solar neutrino data [14]. One can reproduce the nonmonotonic energy dependence of the suppression rate by assuming the half wave-length $\lambda/2$ of eq. (18) to match with the sun-earth distance, i.e.

$$1.25E(\text{MeV})/\delta m^2(\text{eV}^2) \simeq 10^{11}(m), \tag{38}$$

for the middle energy range ($E \sim 5$ MeV). Consequently one gets the best solution for $\delta m^2 \sim 10^{-10}$ eV^2, and a large mixing angle. While the statistical significance of this solution

9

is as good as the small angle MSW, it seems less natural on two counts – the requirement of a large mixing angle and more importantly the fine tuning of the sun-earth distance to match the oscillation length for solar (MeV range) neutrino. Interestingly in this scenario one predicts seasonal variation, due to the eccentricity of earth's orbit, which can be tested by future Super-Kamiokande data. In the absence of such measurement however the vacuum oscillation solution appears less natural than the small angle MSW solution.

Atmospheric Neutrino Oscillation :

The source of atmospheric neutrinos is the decay of $\pi^{\pm}$, which are produced by the collision of cosmic rays with the atmosphere, i.e.

$$
\begin{aligned}
\pi^+ &\rightarrow \mu^+ \nu_\mu, \ \mu^+ \rightarrow e^+ \nu_e \bar{\nu}_\mu; \\
\pi^- &\rightarrow \mu^- \bar{\nu}_\mu, \ \mu^- \rightarrow e^- \bar{\nu}_e \nu_\mu.
\end{aligned}
\tag{39}
$$

Thus one expects a ratio of

$$
R = \frac{\nu_\mu + \bar{\nu}_\mu}{\nu_e + \bar{\nu}_e} = 2.
\tag{40}
$$

The observed ratio is significantly smaller – close to 1 is some situations.

In this case the (Super) Kamiokande is clearly the market leader [15], although there is corroborative evidence from several other experiments [16]. Interestingly the Kamiokande (as well as its super version) started as Kamioka nucleon decay experiment and ended up as Kamioka neutrino detection experiment. In the process it showed that, contrary to the conventional wisdom, yesterday's background can become today's signal. The atmospheric neutrinos have been long recognised to constitute the irreducible background to proton decay. Because of this no earth-based experiment can probe proton life-time beyond 10^{34} years, for which one has to go to the moon. What the (Super) Kamioka experiment did instead was to concentrate on the study of this background. And in the process they seem to have discovered a result, which could be as significant as proton decay.

The two main features of the SK data are as follows.

i) It shows a deficit in the $(\nu_\mu + \bar{\nu}_\mu)$ flux while the $(\nu_e + \bar{\nu}_e)$ flux agrees with the prediction. This favours $\nu_\mu \rightarrow \nu_\tau$ oscillation over $\nu_\mu \rightarrow \nu_e$, which is also supported by the CHOOZ reactor data [17].

ii) The deficit is seen mainly for up-ward going ν_μ, $\cos \Theta < 0$, where capital Θ denotes the zenith angle (to avoid confusion with the mixing angle θ). Note that the distance travelled by the up-ward going neutrino is related to earth's diameter d ($\sim 10^4$ Km) by

$$
\ell = d |\cos \Theta|,
\tag{41}
$$

while that of down-ward going ones is restricted to the atmospheric depth (~ 10 Km). Hence this result suggest the oscillation length ($\lambda/2$) to be of similar order as d.

Fig. 6 shows the zenith angle distribution of the electron and muon neutrinos for different ranges of energy. The theoretical expectations without and with ($\nu_\mu \rightarrow \nu_\tau$) oscillation are

shown by hatched and solid lines respectively. There is no evidence for oscillation in the ν_e case. But there is a clear deficit of ν_μ flux from the no oscillation prediction. The lowest energy bin, corresponding to low oscillation length $\lambda/2 \ll d$, shows a roughly constant deficit as expected from (19) and (41). On the other hand multi-GeV neutrinos correspond to higher oscillation length (18), i.e $\frac{\lambda}{2} \sim d$. In this case the deficit increases steadily with the zenith angle, again in agreement with (19) and (41).

Fig. 7 combines the data points from different zenith angles (41) and energy to give the distribution in the ratio ℓ/E. This is the appropriate quantity for studying the oscillation phenomenon via (17). One sees a large decrease in the ν_μ flux, relative to the Monte Carlo prediction, by almost a factor of 2 as $\ell/E \to 10^3$ Km/GeV. It corresponds to a large mixing angle ($\sin^2 2\theta \sim 1$) and a $\delta m^2 \sim 10^{-3}$ eV^2. Indeed the best solution represented by the dashed line, corresponds to $\sin^2 2\theta = 1$ and $\delta m^2 = 2.2 \times 10^{-3}$ eV^2.

Finally Fig. 8 shows the allowed region of the vacuum oscillation solution to the Super-Kamiokande data in the $\sin^2 2\theta$ and δm^2. The corresponding 90% CL contour of the earlier Kamiokande data is also shown for comparison. Although the latter is slightly higher in δm^2, the two agree within 1.5σ. Of course the combined 90% CL contour will be close to the SK contour because of its higher statistical significance, i.e.

$$\sin^2 2\theta_{\mu\tau} > 0.82 (\theta_{\mu\tau} = 45 \pm 13^0), \tag{42}$$

and

$$\delta m^2 = (0.5 - 6)10^{-3} \text{ eV}^2. \tag{43}$$

Reconciling Large Mixing with Hierarchical Masses :

Thus the atmospheric neutrino oscillation data implies nearly maximal mixing between ν_μ and ν_τ (42). This would normally suggest a degenerate pair of neutrinos, with a small mass difference given by (43). For example a Dirac mass-matrix for the $\nu_\mu - \nu_\tau$ pair would correspond to degenerate masses and maximal mixing, i.e.

$$\begin{pmatrix} 0 & M \\ M & 0 \end{pmatrix} \to \begin{pmatrix} M & 0 \\ 0 & -M \end{pmatrix}, \theta = 45°. \tag{44}$$

However the favoured solution to the solar neutrino oscillation data (Fig. 4) would then require the ν_e to have even a more precise mass degeneracy with one of these states with

$$\delta m^2 = (0.5 - 1)10^{-5} \text{ eV}^2 \tag{45}$$

and

$$\sin^2 2\theta_e = 10^{-3} - 10^{-2} \left(\sin \theta_e = \frac{1}{50} - \frac{1}{20} \right). \tag{46}$$

Such a degeneracy would of course be totally unexpected. It is therefore more natural to consider the alternative of hierarchical neutrino masses instead of degenerate ones. It implies that the two larger mass eigen values correspond to the square-roots of eq. (43) and (45),

$$m_1 \sim 0.05 \text{ eV}, \ m_2 \sim 0.003 \text{ eV}, \tag{47}$$

11

with $m_3 \ll m_2$. Indeed as far as the atmospheric and solar neutrino oscillation phenomena are concerned one can take m_3 to be exactly 0. Note that the m_1 and m_2 mass eigen states correspond to large admixtures of ν_μ and ν_τ (42), with a small ν_e component corresponding to (46).

There is a broad consensus in the current literature in favour of this second alternative. Indeed much of it is devoted to exploring models for reconciling hierarchical masses with at least one large mixing angle. I shall conclude by briefly discussing a minimal see-saw model where the two can be naturally reconciled.

Recall that the canonical see-saw model [2] is based on a $U(1)$ extension of the SM gauge group, corresponding to the gauge charge $B-L$. The latter treats the three neutrino flavours identically, while the atmospheric and solar neutrino oscillation data seem to distinguish the ν_e from ν_μ and ν_τ. Thus to account for these oscillation data one needs to consider a variation of this see-saw model, where the above distinction between the neutrino flavours is incorporated into the choice of the $U(1)$ gauge charge. Two such variations were presented by us in [18] and [19]. I shall concentrate on the latter, because it is more economical. It corresponds to the $U(1)$ gauge charge

$$Y' = B - \frac{3}{2}(L_\mu + L_\tau). \tag{48}$$

The requirement of anomaly cancellation implies two right-handed singlet neutrinos $N_{1,2}$ with $Y' = -3/2$ to match the two doublet ones, carrying this gauge charge.

The minimal Higgs sector consists of

$$\begin{pmatrix} \phi^+ \\ \phi^0 \end{pmatrix}_{Y'=0} \quad \& \quad \chi^0_{Y'=3} \tag{49}$$

as in the canonical see-saw model. The latter acquires a large vev at the Y' breaking scale giving large Majorana masses to $N_{1,2}$, i.e.

$$M_{1,2} \sim \langle \chi \rangle. \tag{50}$$

The ϕ couples these right-handed singlet neutrinos to ν_μ and ν_τ giving them Dirac masses,

$$f\phi\bar{\nu}_{\mu,\tau}N_{1,2} \rightarrow f\langle\phi\rangle\bar{\nu}_{\mu,\tau}N_{1,2}, \tag{51}$$

while there is no such coupling to ν_e. Thus it implies two non-zero mass eigen states of the SM neutrinos, corresponding to large admixtures of ν_μ and ν_τ but no ν_e component. In order to introduce a small mixing of ν_e with these states, as required by the solar neutrino oscillation data, we expand the Higgs sector by an additional doublet and a singlet,

$$\begin{pmatrix} \eta^+ \\ \eta_0 \end{pmatrix}_{Y'=-3/2} \quad \& \quad \zeta^0_{Y'=-3/2}. \tag{52}$$

The doublet introduces a small Dirac coupling of ν_e with $N_{1,2}$ via

$$f\eta\bar{\nu}_e N_{1,2} \rightarrow f\langle\eta\rangle\bar{\nu}_e N_{1,2}. \tag{53}$$

The singlet ζ^0 is required to avoid an unwanted pseudo-Goldstone boson. This comes about because there are three global $U(1)$ symmetries, corresponding to rotating the phases of ϕ, η and χ^0 in the Higgs potential, while only two local $U(1)$ symmetries get broken. The addition of the singlet ζ^0 introduces two more terms in the Higgs potential, $\eta^\dagger \phi \zeta^0$ and $\chi^0 \zeta^0 \zeta^0$, so that the extra global symmetry is avoided.

The doublet η can acquire a small but nonzero vev at the $SU(2)$ breaking scale, which can be estimated from the relevant part of the Higgs potential,

$$m_\eta^2 \eta^+ \eta + \lambda(\eta^\dagger \eta)(\chi^\dagger \chi) + \lambda'(\eta^\dagger \eta)(\zeta^\dagger \zeta) - \mu \eta^\dagger \phi \zeta. \tag{54}$$

Although m_η^2 is positive, after minimisation of the potential we find this field has acquired a small vev,

$$\langle \eta \rangle = \mu \langle \phi \rangle \langle \zeta \rangle / M_\eta^2, \tag{55}$$

where $M_\eta^2 = m_\eta^2 + \lambda \langle \chi \rangle^2 + \lambda' \langle \zeta \rangle^2$ represents the physical mass of η and $\mu \lesssim \langle \zeta \rangle \sim \langle \chi \rangle$. Thus a reasonable choice of $M_\eta \sim 5\langle \zeta \rangle$ implies

$$\langle \eta \rangle / \langle \phi \rangle \sim 1/25, \tag{56}$$

which would correspond to the required mixing angle for ν_e (46).

Let us write down the full 5×5 mass matrix in the flavour basis of $\nu_{e,\mu,\tau}$, corresponding to the mass basis of the charged leptons. Since the latter do not interact with the singlet neutrinos $N_{1,2}$ they can be simultaneously diagonalised in the same basis. Thus we have the symmetric mass matrix

$$\begin{pmatrix} 0 & \cdot & \cdot & \cdot & \cdot \\ 0 & 0 & \cdot & \cdot & \cdot \\ 0 & 0 & 0 & \cdot & \cdot \\ f_e^1 \langle \eta \rangle & f_\mu^1 \langle \phi \rangle & f_\tau^1 \langle \phi \rangle & M_1 & \cdot \\ f_e^2 \langle \eta \rangle & f_\mu^2 \langle \phi \rangle & f_\tau^2 \langle \phi \rangle & 0 & M_2 \end{pmatrix}. \tag{57}$$

We assume the Higgs Yukawa couplings to be of similar magnitude, which means that a mass-matrix arising from a single Higgs vev has a democratic texture. On the other hand, in analogy with the charged leptons, it is reasonable to assume a mild hierarchy for the $N_{1,2}$ mass eigen values, i.e.

$$M_1/M_2 \sim 1/20. \tag{58}$$

There is of course no conflict between the two assumptions; rather they are closely connected. Democratic mass matrices naturally lead to large cancellations in the determinant, which are required for hierarchical mass eigen values.

One can write down the 3×3 mass-matrix for the SM neutrinos from (57) using the see-saw formula [19]. Instead of doing that, we will simply read off the rough magnitudes of the masses and mixings from the matrix elements of (57). We get

$$\begin{aligned} \tan \theta_{\mu\tau} &\sim & f_\mu^1/f_\tau^1 \sim 1, \\ \sin \theta_e &\sim & \langle \eta \rangle / \langle \phi \rangle \sim 1/25, \\ m_2/m_1 &\sim & M_1/M_2 \sim 1/20, \end{aligned} \tag{59}$$

which are in good agreement with the experimental value of (42), (46) and (47). Finally the scale of the $U(1)_{Y'}$ symmetry breaking can be estimated from the see-saw formula,

$$
\begin{aligned}
M_2 = f^2 \langle \phi \rangle^2 / m_2 &= f^2 10^{16} \text{ GeV} \\
&= 10^{12} - 10^{16} \text{ GeV}, \quad (60)
\end{aligned}
$$

depending on whether we take the ϕ Yukawa coupling as $f \sim 10^{-2}$ in analogy with the τ lepton or ~ 1 in analogy with top quark. Thus for a $U(1)_{Y'}$ symmetry breaking scale of $10^{12} - 10^{16}$ GeV the model can naturally account for the large (small) mixing solutions to the atmospheric (solar) neutrino oscillation data.

Let me mention here that there is one more evidence of neutrino oscillation, from the Los Alamos accelerator neutrino experiment [20], which is far more controversial however than the solar and atmospheric neutrino results. If confirmed, it will be hard to explain all the three oscillation results within the framework of three light neutrinos.

I thank Girish Ogale for typing the manuscript and Rajan Pawar for drafting the 1st figure.

References

1. M. Gell-Mann, P. Ramond and R. Slansky, in Supergravity, Proceedings of the Workshop, Stony Brook, New York, 1979 (North-Holland, Amsterdam); T. Yanagida, in Proceedings of the Workshop on Unified Theories and Baryon Number in the Universe, Tsukuba, Japan (KEK Report No. 79-18) 1979.

2. R.E. Marshak and R.N. Mohapatra, Phys. Lett. B91, 222 (1980).

3. B. Pontecorvo, JETP 33, 549 (1957); 34, 247 (1958); 53, 1717 (1967).

4. S.P. Mikheyev and A.Y. Smirnov, Yad. Fiz. 42, 1441 (1985); Nuovo Cim. 9C, 17 (1986).

5. L. Wolfenstein, Phys. Rev. D17, 2369 (1978).

6. H. Bethe, Phys. Rev. Lett. 56, 1305 (1986).

7. See e.g. K. Whisnant, Ashland 1987, Proceedings of Neutrino Masses and Neutrino Astrophysics.

8. S.J. Parke, Phys. Rev. Lett. 57, 1275 (1986); S.J. Parke and T.P. Walker, Phys. Rev. Lett. 57, 2322 (1986).

9. S.T. Petcov, hep-ph/9806466; J.N. Bahcall, Neutrino Astrophysics, Cambridge University Press, Cambridge, 1989.

10. GALLEX Collaboration: W. Hampel et. al., Phys. Lett. B388, 364 (1996); SAGE Collaboration: V. Garvin et. al., Neutrino-98, Takayama, Japan (1998).

11. Homestake Expt.: B.T. Cleveland et. al., Astrophys. J. 496, 505 (1998); R. Davis, Prog. Part. Nucl. Phys. 32, 13 (1994).

12. Kamiokande Collaboration: K.S. Hirata et. al., Phys. Rev. Lett. 77, 1683 (1996); Super-Kamiokande Collaboration: Y. Suzuki, Neutrino-98, Takayama, Japan (1998).

13. N. Hata and P.G. Langacker, Phys. Rev. D56, 6107 (1997).

14. J.N. Bahcall, P.J. Krastev and A.Y. Smirnov, Phys. Rev. D58, 096016 (1998).

15. Kamiokande Collaboration: Y. Fukuda et. al., Phys. Lett. B335, 237 (1994); Super-Kamiokande Collaboration: Phys. Rev. Lett. 81, 1562 (1998).

16. IMB Collaboration: R. Becker-Szendy et. al., Nucl. Phys. (Proc. Suppl.) 38, 331 (1995); Soudan-2 Expt.: W.W.M. Allison et. al., hep-ex/9901024.

17. CHOOZ Collaboration: M. Appollonio et. al., Phys. Lett. B420, 397 (1998).

18. Ernest Ma, D.P. Roy and Utpal Sarkar, Phys. Lett. B444, 391 (1998).

19. Ernest Ma and D.P. Roy, hep-ph/9811266 (to be published in Phys. Rev. D).

20. LSND Collaboration: A. Athanassopoalos et. al., nucl-ex/9706006.
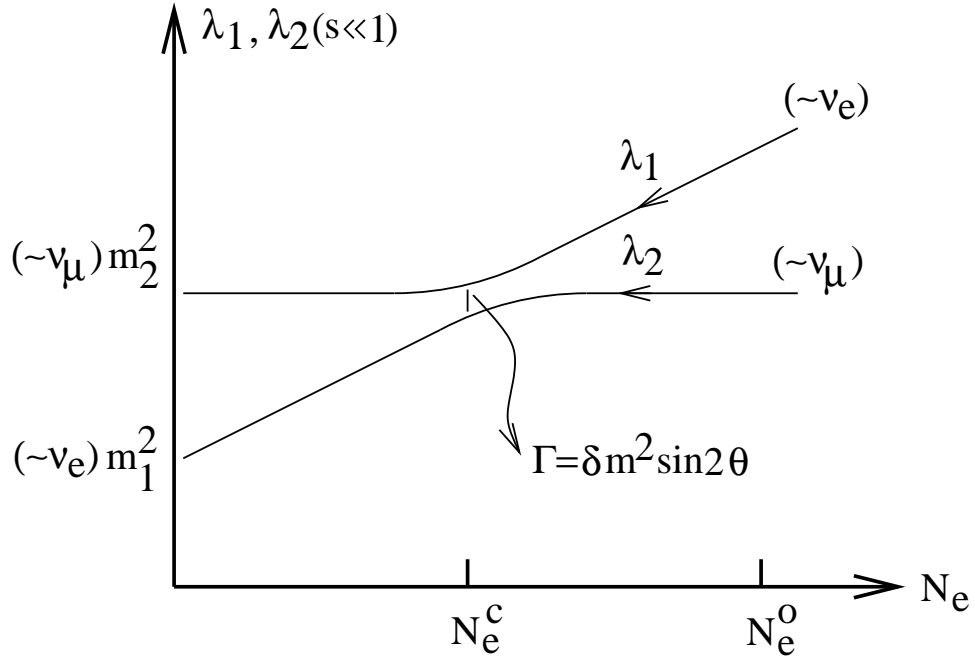
Figure 1: Schematic diagram of the energy eigenvalues of ν_e and ν_μ as functions of electron density; N_e^0 denotes the electron density at the solar core and N_e^c the critical density where the two energy levels cross [6,7].
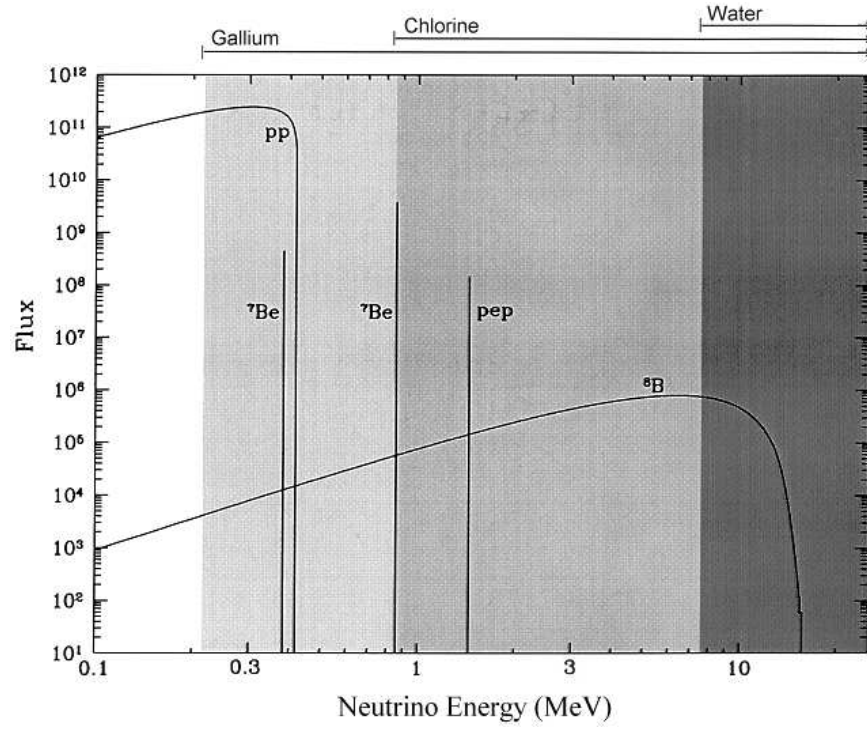
Figure 2: The spectra of the pp, pep, ^7Be and ^8B neutrinos are shown along with the energy ranges of different solar neutrino experiments [9].
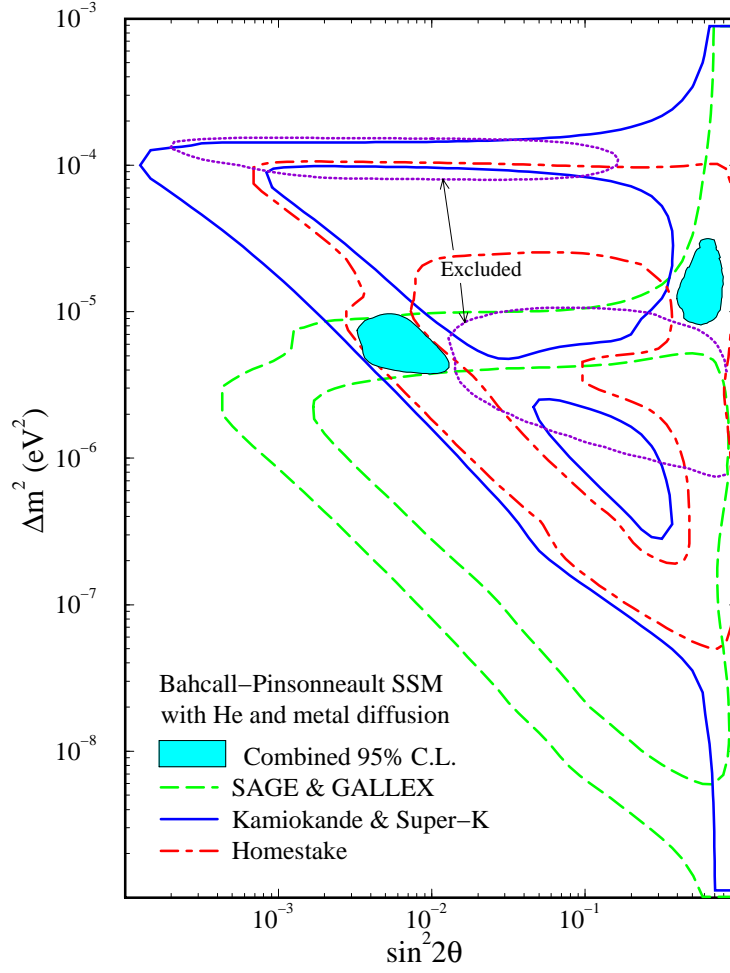
Figure 3: The 95% CL contours of MSW solution for the suppression rates observed by different solar neutrino experiments [13]. Also shown are the regions excluded by the Kamiokande energy spectrum and day-night asymmetry.
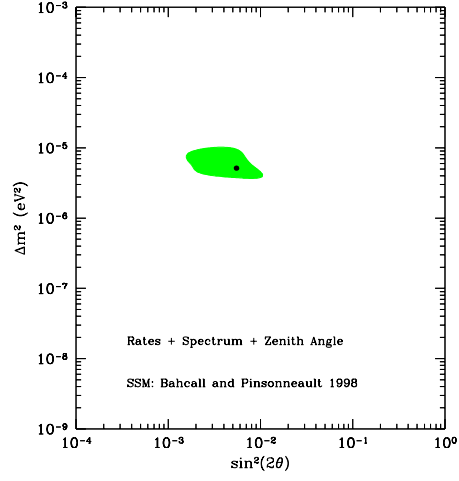
Figure 4: The MSW solution to the combined solar neutrino data on suppression rates along with the Super-Kamiokande energy spectrum and zenith angle distribution. The contour is drawn at 99% CL [14].
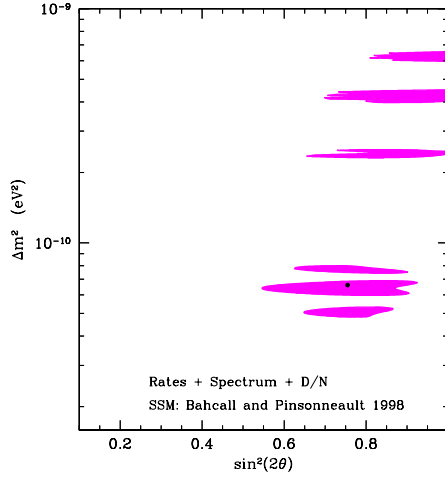
Figure 5: The vacuum oscillation solution to the combined solar neutrino data on suppression rates along with the Super-Kamiokande energy spectrum and day-night asymmetry. The contours are drawn at 99% CL [14].
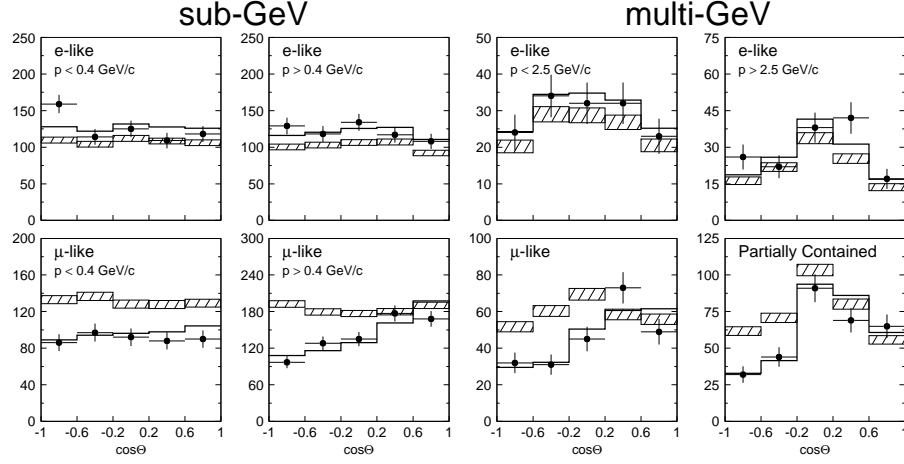
Figure 6: Zenith angle distribution of atmospheric ν_e ($\bar{\nu}_e$) and ν_μ ($\bar{\nu}_\mu$) events from Super-Kaniokande for different energy ranges. The partially contained ν_μ ($\bar{\nu}_\mu$) events roughly correspond to $p > 10\,\text{GeV/c}$. The theoretical prediction with and without $\nu_\mu \to \nu_\tau$ oscillation are shown by solid and hatched lines respectively [15].

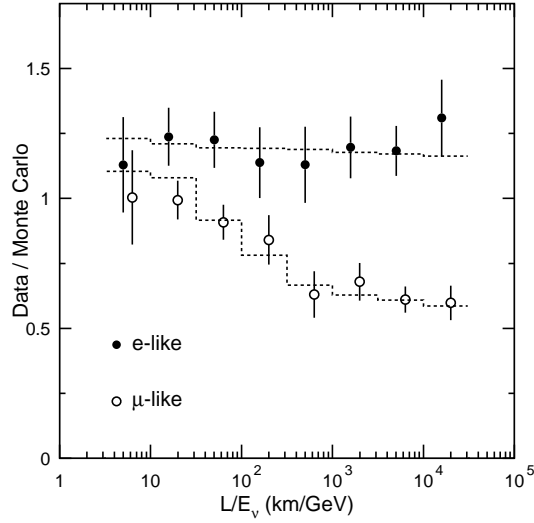Figure 7: The survival probabilities $P_{\nu_e \to \nu_e}$ and $P_{\nu_\mu \to \nu_\mu}$ observed by the Super-Kamiokande atmospheric neutrino experiment are shown against the reconstructed ℓ/E_ν. The theoretical prediction with the without $\nu_\mu \to \nu_\tau$ oscillation are shown by the lower and upper lines respectively [15].
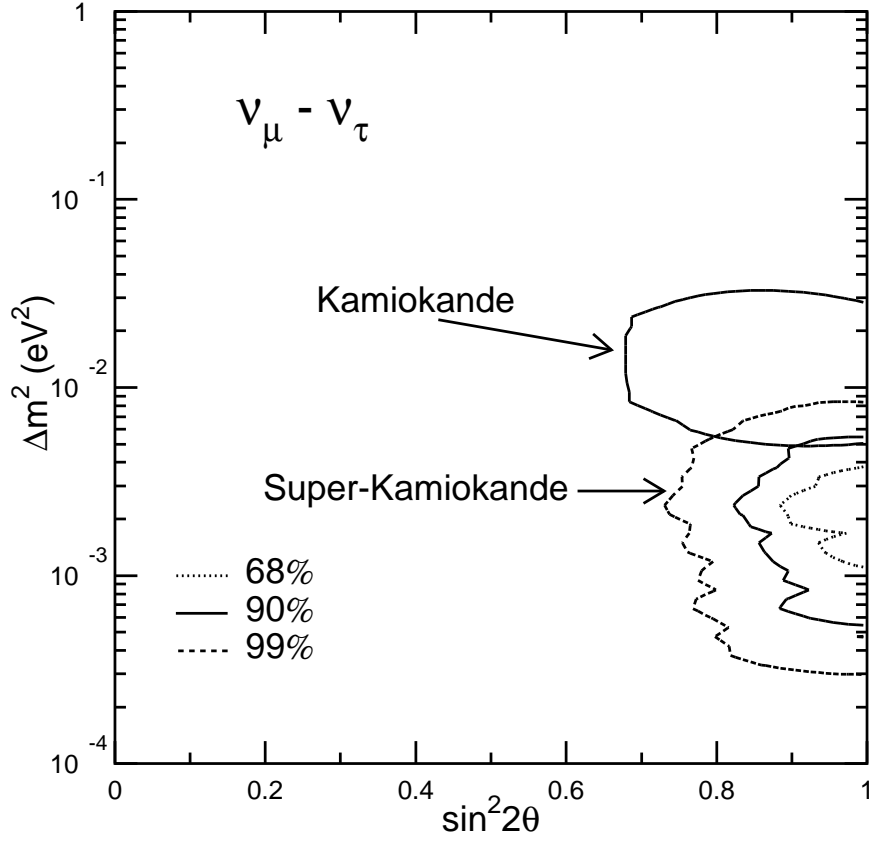
Figure 8: The $\nu_\mu \rightarrow \nu_\tau$ oscillation solutions to the Super-Kamiokande atmospheric neutrino data are shown at 68%, 90% and 99% CL. The corresponding 90% CL contour for the Kamiokande data is also shown for comparison [15].